Validated edge and core predictions of tungsten erosion and transport in JET ELMy H-mode plasmas

OPEN ACCESS
IOP Publishing
Plasma Physics and Controlled Fusion
Plasma Phys. Control. Fusion **66** (2024) 055007 (12pp)
https://doi.org/10.1088/1361-6587/ad3186

Validated edge and core predictions of tungsten erosion and transport in JET ELMy H-mode plasmas

H A Kumpulainen[1,*], M Groth[1], S Brezinsek[2], F Casson[3], G Corrigan[3], L Frassinetti[4], D Harting[2], J Romazanov[2] and JET contributors[5]

[1] Aalto University, Espoo, Finland
[2] Forschungszentrum Jülich GmbH, Jülich, Germany
[3] UKAEA, Culham Science Centre, Abingdon, United Kingdom
[4] Division of Fusion Plasma Physics, KTH, Stockholm, Sweden

E-mail: henri.kumpulainen@aalto.fi

Received 30 September 2023, revised 23 February 2024
Accepted for publication 7 March 2024
Published 20 March 2024

Abstract

Predictive edge and core simulations of tungsten (W) erosion and transport in JET ITER-like wall plasmas are shown to be consistent with the experimentally inferred W density in the main plasma, within the uncertainty inherited from the measurements of the deuterium plasma conditions and from the W density measurements. The ERO2.0 code is applied to predicting the W erosion and edge transport, whereas JINTRAC predicts W transport from the pedestal top to the core plasma. The studied plasma scenarios range from L-mode to the highest-performance deuterium ELMy H-mode in JET.

Keywords: tungsten, erosion, transport, tokamak, edge-localised mode, simulation, validation

1. Introduction

Tungsten (W) is the material choice for the plasma-facing components in many existing and future magnetic confinement fusion devices, as its high resilience to heat, erosion, and fuel retention is advantageous for compatibility with the engineering challenges of a fusion reactor [1, 2]. Contamination of the plasma by eroded W has a strong detrimental impact on fusion performance even at concentrations as low as 10^{-4} due to W spectral line radiation degrading the energy confinement time [3]. Therefore, the ability to understand and predict the erosion and transport of W from the plasma-facing components into the core plasma is critical for designing efficient fusion reactors with W components [4].

In this work, a novel simulation workflow for predicting the W erosion and the resulting W density profile with improved accuracy is described. The work builds upon earlier W modelling and validation studies [5–8] combined with recent development of improved analysis and modelling tools [9–12]. The predictions are validated using measurement data from a variety of Joint European Torus (JET) ITER-like wall (JET-ILW) L-mode and type-I ELMy H-mode discharges.

2. Methods

In this work, W erosion and transport is studied using JINTRAC and ERO2.0 simulations and comparisons with measurements. The JINTRAC suite of codes [13] includes the

[5] See the author list of 'Overview of T and D-T results in JET with ITER-like wall' by C F Maggi *et al* in *Nuclear Fusion Special Issue: Overview and Summary Papers from the 29th Fusion Energy Conf. (London, UK, 16–21 October 2023)*

[*] Author to whom any correspondence should be addressed.

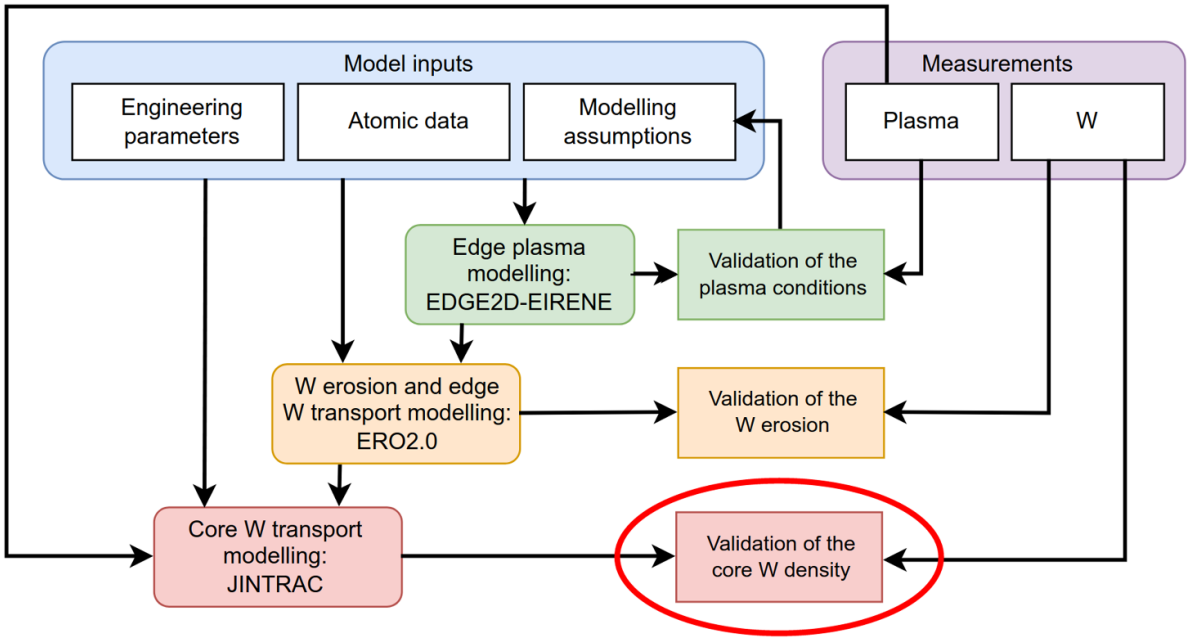

Figure 1. Illustration of the simulation workflow described in this article. The primary focus is analysing and evaluating predictions of W transport and the core W density, as the edge plasma modelling and W erosion steps were presented in an earlier publication [6].

2D multi-fluid edge plasma/kinetic neutral code EDGE2D-EIRENE [14, 15], the 1.5D core transport codes JETTO for main ions and SANCO for impurities, an interface for coupling to higher-dimensional first-principles transport codes such as NEO [16] and QuaLiKiz [17], and other computational tools. ERO2.0 [18] is a 3D full-orbit Monte Carlo trace-impurity code for modelling plasma–wall interactions and impurity transport.

While it is possible to simulate the plasma conditions and the erosion and transport of W simultaneously in a single JINTRAC core–edge integrated simulation, the modelling workflow applied in this work is separated into three stages (figure 1) for several reasons. Firstly, the numerical stability and execution time of the EDGE2D-EIRENE plasma simulations are greatly improved by using ERO2.0 instead of EDGE2D-EIRENE for W erosion and transport. Hence, obtaining converged plasma solutions and iterating them to optimise code-experiment agreement is more feasible when W transport is separated from the EDGE2D-EIRENE simulations.

Secondly, the presented three-stage workflow enables the inclusion of additional physics compared to a single integrated core–edge simulation. For example, JETTO simulations with NEO are challenging to combine with time-dependent edge-localised modes (ELMs) and coupling to EDGE2D-EIRENE. The problem is avoided by using the ELM-averaged W density predicted by ERO2.0 at the pedestal top as the boundary condition to the core W transport simulation. Another example is the inclusion of cross-field drifts in EDGE2D-EIRENE, which is currently infeasible to achieve in ELMy H-modes with W included, but successfully included in this work in an inter-ELM H-mode background plasma without W.

Thirdly, ERO2.0 provides a more complete treatment of plasma–wall interactions than EDGE2D-EIRENE. The presented modelling approach allows simulating material mixing and re-erosion of deposited material from plasma-facing components, accounting for incidence angles in sputtering yield calculations, and applying a more detailed 3D geometry of the wall components than the axisymmetric limiter and divertor contour in EDGE2D-EIRENE. EIRENE accounts for the incidence angles of neutral particles in erosion yield calculations, but the ions from EDGE2D are not tracked particles in EIRENE. Nearly perpendicular incidence is assumed for ions in EDGE2D-EIRENE. In contrast, ERO2.0 has fully resolved incidence angles for traced ions and atoms, and prescribed (not necessarily perpendicular) incidence angles for the imported background plasma.

Furthermore, the full-orbit kinetic transport model of ERO2.0 is more complete than the multi-fluid treatment of W in JINTRAC. The neoclassical cross-field transport of W is inherently included in ERO2.0 without compromising the computational time or stability, unlike in EDGE2D-EIRENE.

To separate the uncertainty of predicting W erosion and transport from the uncertainties in predicting the plasma conditions, the background plasma simulations are extensively fitted for optimal agreement with available measurements. Nevertheless, the uncertainties due to the background plasma conditions constitute most of the estimated total uncertainty in the W predictions.

No information from any W diagnostics is used to fit the predictive W simulations. Instead, the W measurements are reserved solely for assessing the validity of the simulations.

Table 1. Summary of the studied JET-ILW plasma discharges. The ELM and inter-ELM electron temperatures at the low-field side divertor target ($T_{e,OSP}$) are based on Langmuir probe data when available and predicted (*) by EDGE2D-EIRENE otherwise.

Pulse #	B_T (T)	I_p(MA)	P_{aux} (MW)	$n_{e,ped}$ (m^{-3})	$T_{i,ped}$ (eV)	f_{ELM} (Hz)	$T_{e,OSP}$ (eV)
81 472 (9 s)	2.5	2.5	1	$1.5 \cdot 10^{19}$	650	L-mode	55
82 486 (14 s)	2.0	2.0	10	$6.1 \cdot 10^{19}$	800	28	15–110*
94 606 (10 s)	2.5	2.3	18	$5.3 \cdot 10^{19}$	1100	40	25–180*
97 781 (9 s)	3.45	2.3	34	$4.2 \cdot 10^{19}$	3500	40	80*–600*

2.1. JET plasma discharges

The four plasma scenarios studied in this work include one low-recycling L-mode and three type-I ELMy H-modes ranging from relatively high electron density and low fusion performance to the JET hybrid discharge with a record-high sustained D–D fusion rate [19] (table 1). The choice of plasma scenarios is mainly influenced by the available diagnostic coverage and quality of each plasma discharge, the range of engineering parameters and plasma conditions covered by the scenarios, as well as the applicability of pre-existing background plasma simulations to accelerate the modelling schedule. The studied time interval from each discharge is selected for the steadiest obtainable plasma conditions and diagnostic availability.

2.2. Background plasma simulations

The time-evolution of the plasma parameters at each phase of the ELM cycle is simulated in JINTRAC with an imposed ELM frequency and *ad-hoc* heat and particle transport multipliers, adjusting the free parameters to reproduce the measured time-evolution of both the pedestal and the divertor conditions as closely as possible. The measured quantities used in the validation of the simulated ELM cycle include the ELM energy loss, the ELM frequency, the pre-ELM and post-ELM electron density and temperature profiles along the outer mid-plane, and the ELM power load incident on the low-field side target. Additionally, the cross-field heat and particle transport coefficients are iteratively adjusted to reproduce the inter-ELM electron density, electron temperature, and ion saturation current profiles along the low-field side target as measured by Langmuir probes. The simulated D_2 fuelling rate and the heating power are consistent with the experiments.

The background plasmas for ERO2.0 are created from snapshots of the pre-ELM, intra-ELM, and post-ELM phases from the time-dependent JINTRAC simulations. In scenarios with negligible differences between post-ELM and pre-ELM scrape-off layer (SOL) conditions, a single background plasma represents the entire inter-ELM phase.

In addition to ELMs altering the deuterium plasma conditions, the direct impact of ELMs on W transport (ELM flushing) is simulated as a prescribed anomalous radial outward convective velocity, which is calculated from the measured loss rate of plasma stored energy during ELMs. By assuming that both W and the fuel ions are collectively expelled from the pedestal by ELMs at the same velocity, and that ELMs induce ballooning radial transport proportional to B_T^{-2} primarily on the low-field side, the effective contribution of ELMs to the radial velocity of W across the separatrix is estimated as:

$$v_{rad,W,sep}(R,t) = \frac{P_{loss,ELM}(t)}{\frac{3}{2} n_{e,ped} k (T_{e,ped} + T_{i,ped}) A_{LCFS}} \frac{R^2}{\langle R^2 \rangle}. \quad (1)$$

The intra-ELM energy loss rate $P_{loss,ELM}$, the area of the last closed flux surface A_{LCFS}, and the flux-surface-averaged major radius squared $\langle R^2 \rangle$ are based on pressure-constrained magnetic equilibrium reconstruction (EFTP), whereas $n_{e,ped}$ and $T_{e,ped}$ are based on high-resolution Thomson scattering measurements and $T_{i,ped}$ on charge-exchange recombination spectroscopy. The ELM-affected region is assumed to be flux surfaces with normalised minor radius ρ between 0.9 and 1, linearly interpolating the radial convective velocity between 0 at $\rho = 0.9$ and $v_{rad,W,sep}$ at the separatrix.

The intra-ELM phase begins with the ELM crash, during which the energy loss rate reaches its maximum for a duration of <0.5 ms. The ELM crash is followed by the several times longer ELM decay phase, during which the energy loss and therefore also the estimated $v_{rad,W,sep}$ are decreasing while the heat fluxes in the SOL remain several times above the inter-ELM level.

2.3. Simulating W transport in the edge plasma

The ERO2.0 simulations of W erosion and edge transport are based on earlier ERO2.0 studies which validate the predicted W erosion rate in the low-field side divertor using W I spectroscopy [6]. The predominant causes of the predicted W sputtering are D ions during ELMs and Be ions between ELMs, concentrated near the strike lines, consistent with analysis of JET experiments [20]. W erosion by D atoms is predicted to be a negligible fraction of the gross W source at the divertor targets, but the main cause of W erosion in non-plasma-wetted regions, adding up to 5%–15% of the total W gross erosion distributed across the entire divertor area. W sputtering by D ions and atoms is predicted by ERO2.0 based on imported JINTRAC and EIRENE solutions respectively, whereas W sputtering by Be and W self-sputtering predictions are based on particle trajectories followed in the preceding time step of the ERO2.0 simulation. W self-sputtering contributes 3%–20% of the predicted W gross erosion, mostly during ELMs. Seeding impurities are not considered a relevant cause of W sputtering in the studied scenarios.

Material mixing is included in the presented ERO2.0 simulations, and it reduces the W erosion yield especially on the JET high-field side divertor shoulder, which is covered by a beryllium-rich deposit layer [6]. The sources of Be in the ERO2.0 simulations include erosion from the main chamber Be components and re-erosion from all plasma-facing surfaces due to sputtering by D, Be, and W ions and atoms, primarily D ions. Ion fluxes to the main chamber surfaces are estimated by extrapolating the JINTRAC plasma solution in the radial direction with exponentially decaying density and temperature profiles. The divertor W targets are assumed to have a Be surface concentration (up to 30%) sufficient to reproduce the experimentally inferred Be density in the divertor plasma [6]. The simulated Be concentration is validated by comparing ERO2.0 synthetic diagnostics of Be II line emission with the 527 nm Be II emission profiles measured in the low-field side divertor.

In the ERO2.0 simulations of ELMy H-mode plasmas, the eroded W atoms and ions are traced for 0.5 ms at a time, after which the state of the W particle markers is saved into a file. ERO2.0 is then executed again with updated plasma conditions, the previously non-deposited W markers are imported from the saved file, and the simulation is continued with a combination of newly eroded W and markers resumed from the previous time step. Several complete ELM cycles are simulated until an approximate periodic dynamic equilibrium is reached.

Thermal forces [10, 21] and electric fields are included in all presented ERO2.0 simulations. Anomalous cross-field diffusion and convection are for the first time imposed as 2D profiles based on JINTRAC predictions, as opposed to previous ERO2.0 simulations with spatially constant anomalous diffusivity.

As part of these studies, the parallel-**B** effects of plasma rotation were newly implemented in ERO2.0 and confirmed to accurately reproduce the observed poloidal W asymmetry in experiments. A more complete ERO2.0 implementation of plasma rotation, also including its effects on cross-field transport, is expected in the future. Until then, the contribution of rotation to neoclassical cross-field W transport is calculated in the preprocessing phase using the FACIT tool [11] and prescribed in ERO2.0 as a 1D radial profile.

The assumption of a Maxwellian distribution of atom impact energies in sputtering yield calculations in ERO2.0 [6] is replaced with kinetic atom impact energy spectra extracted from standalone EIRENE simulations. The ability to import and apply spatially resolved impact energy spectra was newly implemented in ERO2.0. The Maxwellian assumption is found to be invalid in the energy range relevant for W sputtering by D atoms (>300 eV) due to a non-Maxwellian high-energy tail created by charge-exchange reactions (figure 2). Calculations using the kinetic energy spectra predict up to 1–2 orders of magnitude more sputtering of W by D atoms compared to the Maxwellian assumption.

2.4. Simulating W transport in the core plasma

The modelling approach for W on the closed flux surfaces inside $\rho = 0.9$, using JETTO and SANCO coupled with NEO, is based on earlier validation studies of core W transport [8]. The most notable difference compared to the earlier work is that the total W content is no longer a fitting parameter, but a prediction from the ERO2.0 and JINTRAC simulations. Converged core plasma solutions are initially obtained using fast Bohm–gyro-Bohm [22] anomalous transport and NCLASS [23] neoclassical transport models, then validated against the measured ion and electron temperature and density profiles. The Bohm and gyro-Bohm terms for ions and electrons are scaled by *ad-hoc* factors and the simulation is iterated until the measured plasma profiles are closely reproduced. The plasma rotation frequency and the total radiated power are prescribed to their measured values, and for computational stability reasons the predicted W radiation is only used post-simulation to assess self-consistency. The background plasma simulations are fitted to the extent justified by the background plasma measurements, but the simulations are not adjusted to match the predicted W density or W radiation to any measurements. The workflow for W is fully predictive in the sense that the W sources, the W transport models, and the predicted W density are not fitted. The converged simulations are continued with the computationally more expensive higher-fidelity transport models NEO and QuaLiKiz neural network (QLK-NN) [12] for W neoclassical and turbulent transport respectively, to improve the accuracy of the predictions and to include the impact of plasma rotation on neoclassical W transport. The boundary condition for the W density is the ELM-averaged and flux-surface-averaged ERO2.0 prediction at normalised minor radius $\rho = 0.9$.

3. Predicted erosion and edge transport of W

3.1. Comparison of divertor screening by W source location

ERO2.0 predicts that W sources in the JET divertor near the strike lines and in the high-field side SOL result in negligible W influx to the main plasma, whereas W sources near and above the low-field side divertor entrance are poorly screened from the main plasma (figure 3). To compare the screening efficiency of W source locations in the divertor, sputtering was disabled and a toroidally localised artificial point source of W was placed at various divertor locations in each simulation case. The magnitude of the W source in each case was equal (10^{20} atoms s^{-1}) with an initial energy of 10 eV. Screening at the divertor targets is predicted to be virtually perfect even when the initial W energy is set to an exceptionally high value of 100 eV. When the W influx due to each point source is weighted by the predicted W erosion rate in the corresponding divertor region, W eroded from the low-field side divertor shoulder explains 80%–95% of the predicted W in the main plasma.

The reasons contributing to the poor W screening at the low-field side divertor entrance include (a) a long ionisation mean-free path of W and (b) a low probability of prompt redeposition, both due to the low electron density and temperature. (c) The stagnation front of the main ion flow is predicted near the W sources, hence the friction between W and main ions does not provide strong W screening, unlike near the targets

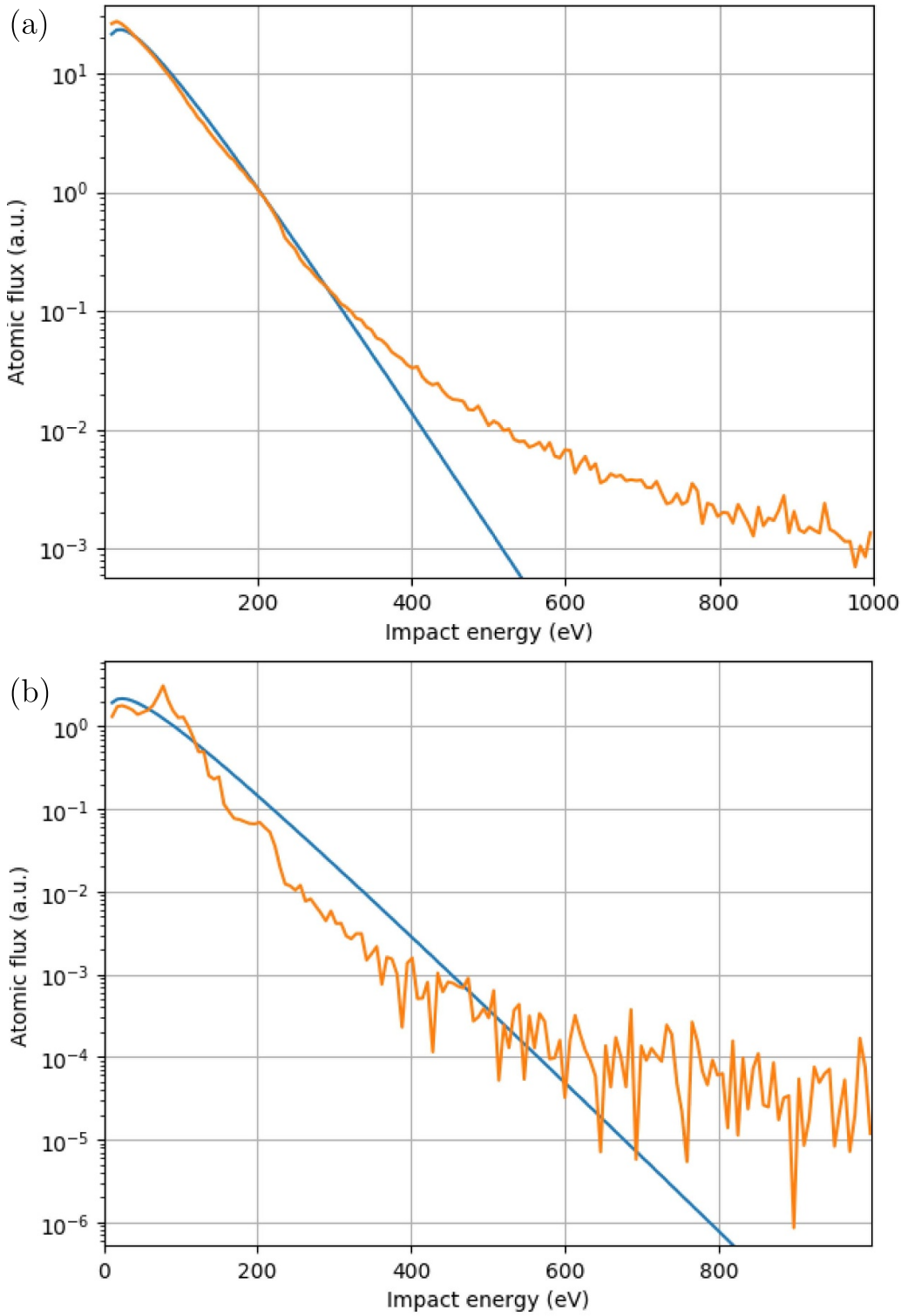

Figure 2. The impact energy spectrum of D atoms incident on (a) the low-field side (horizontal) target and (b) a similar-area section from the low-field side vertical divertor, calculated using EIRENE (orange) based on a JINTRAC plasma solution representing L-mode JET pulse #81 472 at 9 s. A Maxwellian energy distribution with the same mean energy as the kinetic spectrum, (a) 64 eV and (b) 154 eV, is shown in blue for comparison.

and in the high-field side far SOL. (d) The W screening by the pre-sheath parallel-**B** electric field is weak due to the lack of significant plasma wetting on components at the low-field side divertor entrance.

3.2. ELM-resolved time evolution of the W density

In JET hybrid scenario plasmas with maximum available heating power and relatively low edge density, ERO2.0 predicts the

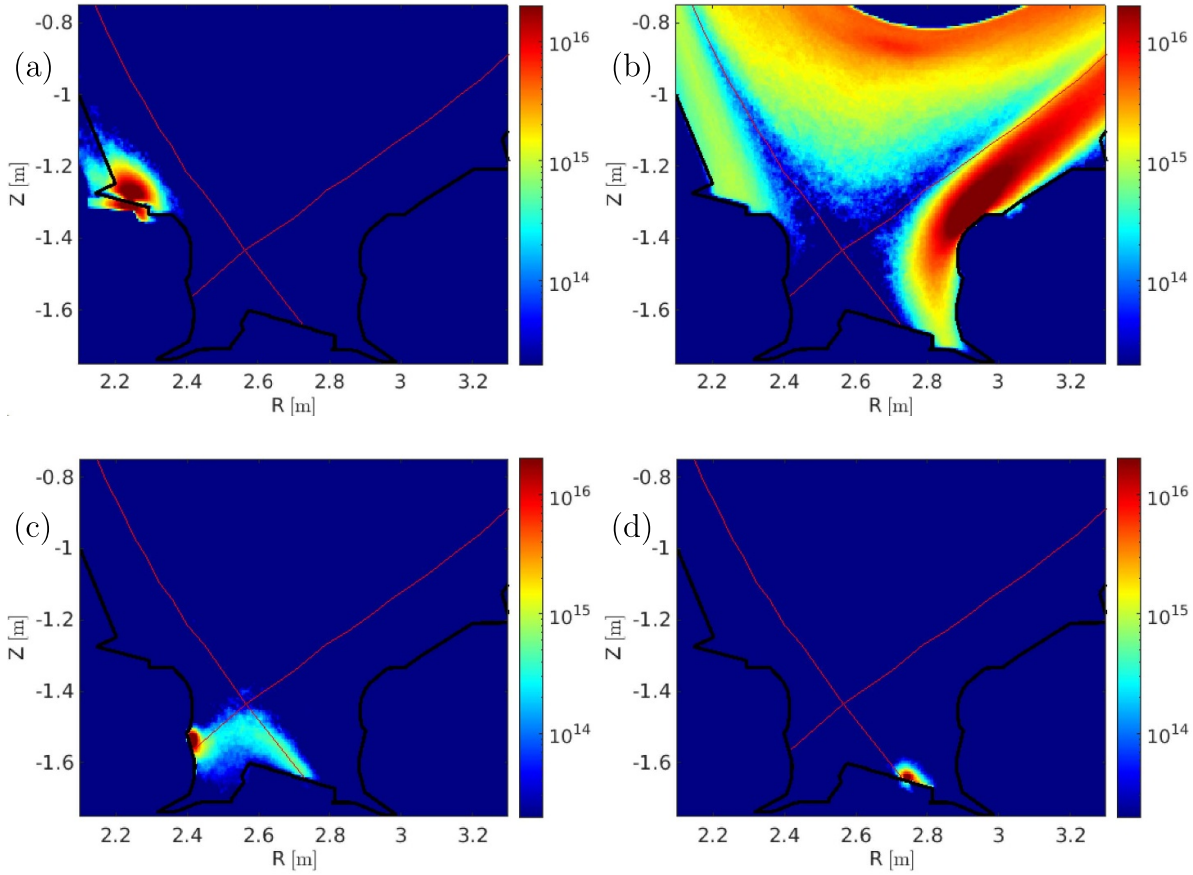

Figure 3. Poloidal cross-section of the W density profile (m^{-3}) predicted by ERO2.0 due to a point source of W (a) in the high-field side far SOL, (b) at the low-field side divertor entrance, (c) at the high-field side target, and (d) at the low-field side target. The study was repeated for 15 W source locations in L-mode as well as inter-ELM and intra-ELM H-mode plasmas, out of which four representative L-mode cases are shown.

W density in the confined plasma to increase during the post-ELM phase, reaching a maximum and decreasing in the pre-ELM phase (figure 4(a)). The ELM description applied in the background plasma simulations is simplistic (section 2.2), but the plasma solutions are optimised to reproduce the measured conditions in each phase of the ELM cycle. The reversing trend between the post-ELM and pre-ELM phases is explained by outward neoclassical ion temperature screening of W ions in the mantle region ($0.4 < \rho < 0.95$) during the pre-ELM phase, whereas during the post-ELM phase the predicted W neoclassical convection is inward at the pedestal top. Within the edge transport barrier, the predicted neoclassical convection of W is strongly inward during all phases of the ELM cycle. The ERO2.0 predictions are consistent with statistical analysis of the measured evolution of the W content in JET hybrid plasmas [24].

The ELMs induce flushing of W from the main plasma as well as increased W influx due to high erosion. The predicted net effect of ELMs in the hybrid scenario is relatively weak and sensitive to the pre-ELM W density among other factors, hence not determined here with significant confidence.

In contrast to the hybrid scenario, JET type-I ELMy H-mode plasmas with only 10 MW of neutral beam injection (NBI) heating power and a higher electron density are predicted to have a nearly constant inter-ELM W density at the pedestal top (figure 4(b)). The ELMs are predicted as the dominant cause of both W flushing and influx, as the inter-ELM W erosion rate is comparatively low in colder and denser edge plasmas. Due to the strong inward W convection predicted across the pedestal in the inter-ELM phase, the W density eventually reaches a level at which the net effect of ELMs is a reduced W content.

4. Predicted core transport of W

4.1. Flux-surface averaged W density and radiation profiles

JINTRAC predictions of core W transport with a boundary condition based on the ERO2.0 ELM-averaged W density at the pedestal top agree with the experimentally inferred W density profile to less than a factor of 2 in L-mode and a factor of 2 to 3 in ELMy H-mode plasmas (figure 5). The experimentally inferred profiles are based on integrated data analysis of soft x-ray, vacuum-ultraviolet, 2D bolometric, and effective charge measurements, also accounting for light and medium-Z impurities [9].

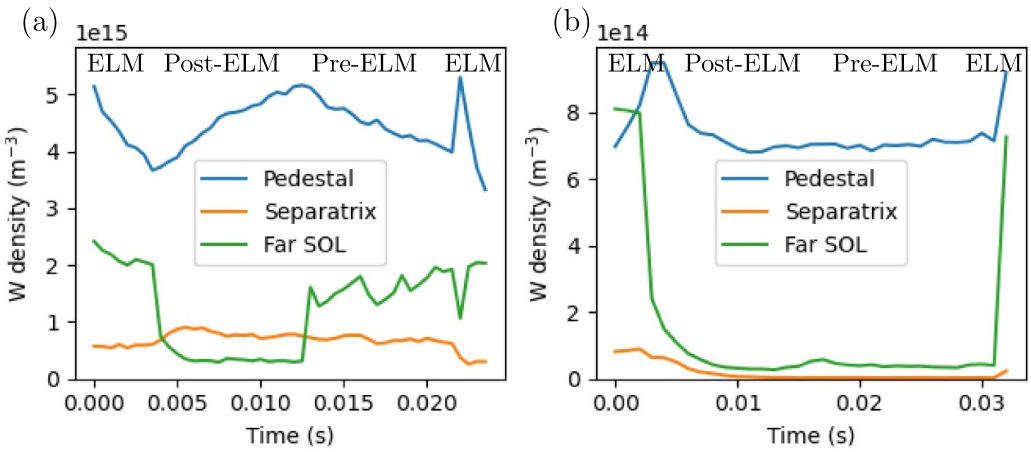

Figure 4. The W density predicted by ERO2.0 at the pedestal top ($\rho = 0.9$, blue), at the separatrix ($\rho = 1$, orange), and in the far scrape-off layer ($\rho = 1.05$, green) as a function of time during an ELM cycle (a) in hybrid H-mode #97 781 (9 s) with $P_{\text{aux}} = 34$ MW and (b) in H-mode #82 486 (14 (s) with $P_{\text{aux}} = 10$ MW.

Flux-surface averaged profiles of the W radiated power density predicted by JINTRAC yield a similar level of agreement with the experimentally inferred W radiation (figure 6) as the W density comparisons. The ratio of predicted to observed W varies by less than 30% between the density and radiation profiles; this is potentially explained by the different assumptions on the W charge state distribution (transport vs. coronal equilibrium) and the different methods of reconstructing the background plasma profiles between the JINTRAC modelling and the measurement analysis. The JINTRAC W radiation profiles are decoupled from the simulated plasma conditions for computational stability, and the total radiated power of the background plasma is prescribed. It is possible to improve simulation self-consistency by including the impact of W radiation on the plasma conditions, but at the expense of simulation accuracy and robustness. When applying the proposed workflow to unexplored scenarios in which the total radiated power is unknown, the impact of the predicted W radiation should be iterated with revised background plasmas for more self-consistent W density and background plasma predictions.

4.2. 2D W density profiles with poloidal asymmetry

The poloidal W asymmetries predicted by both ERO2.0 and JINTRAC (NEO and QLK-NN) are consistent with the observed W radiation asymmetry (figure 7). The ERO2.0 prediction (figure 7(c)) is an average of all time steps during one simulated ELM cycle. To improve the statistical quality of the sampled W distribution in regions of relatively low W gross erosion, the presented ERO2.0 result is a composite consisting of two series of simulations: one with W erosion enabled only at the divertor targets and one with W erosion enabled everywhere else. The main causes of predicted W influx to the confined plasma are the W components near the low-field side divertor entrance. The largest W gross erosion sources at the targets contribute little to the predicted W density due to rapid prompt and non-prompt local redeposition. In the presented hybrid scenario, the ELM-averaged W density in the near-separatrix SOL is one order of magnitude lower than at the pedestal top as a result of fast parallel-**B** SOL transport towards the divertor and inward cross-field neoclassical convection near the separatrix. The W density artifacts visible in the low-field side far SOL near the top of the plasma are induced by gradients in the radially extrapolated background plasma conditions and do not constitute a significant source or sink of W.

The 2D W density profile predicted by JINTRAC (figure 7(b)) is a reconstruction from the radial W density profile predicted on the 1D SANCO grid and the poloidal asymmetry from the higher-dimensional codes NEO and QLK-NN. The flux surfaces up to $\rho = 1$ are visible in the figure, but the W density boundary condition is set to match the flux-surface averaged W density at $\rho = 0.9$ with the ERO2.0 prediction. The part of the JINTRAC W density profile outside $\rho = 0.9$ should be disregarded as the plasma conditions in the JINTRAC core W transport simulation are validated only in the region $0 < \rho < 0.9$.

4.3. Estimated modelling uncertainties

The W density in the core plasma is highly sensitive to the radial gradients of electron density and ion temperature, as well as to the toroidal rotation frequency. The predictive uncertainty of W is reduced by integrated data analysis of several diagnostics, averaging the measured profiles over time, and meticulously adjusting the simulated core plasma profiles to the measurement data. Despite such efforts, the modelling uncertainty in the H-mode W transport simulations due to uncertainties in the simulated plasma conditions on closed flux surfaces is estimated to be approximately a factor of 2 or greater, depending on the scenario. In particular, the edge transport barrier with high gradients is challenging to resolve and reproduce with high precision due to its time evolution and variation among the measured pre-ELM profiles. Quantifying the impact of predicted turbulent W transport on the uncertainty of the W density profiles requires further research, however neoclassical W transport is considered to be the more significant transport mechanism in JET [25].

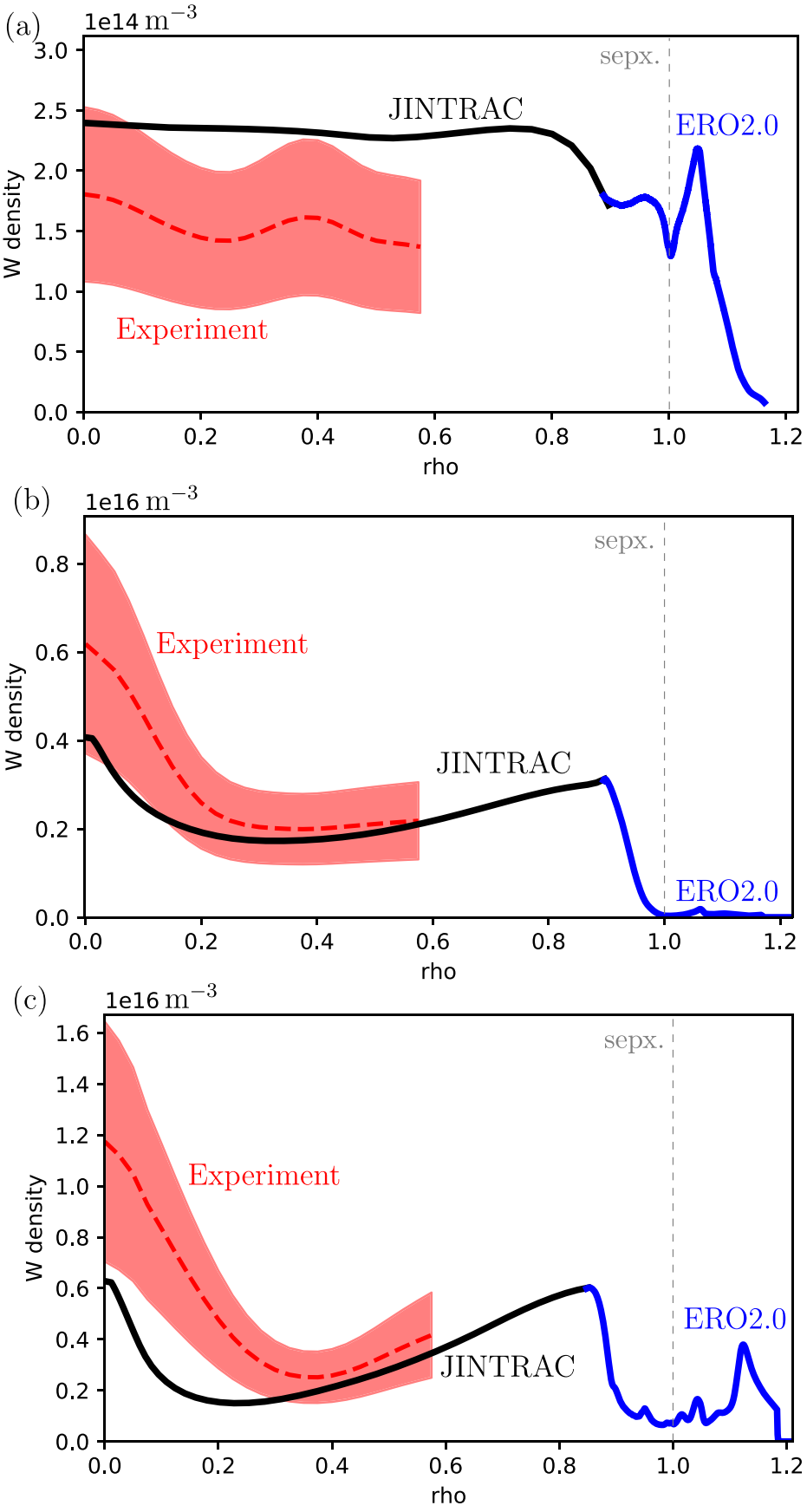

Figure 5. ELM- and flux-surface-averaged W density profiles predicted by ERO2.0 (blue lines) and JINTRAC (black lines) compared to the experimentally inferred W density [9] (red dashed lines with red shaded confidence intervals) as a function of the normalised minor radius in JET (a) L-mode #81 472 at 9 s, (b) ELMy H-mode #94 606 at 10 s, and (c) hybrid ELMy H-mode #97 781 at 9 s.

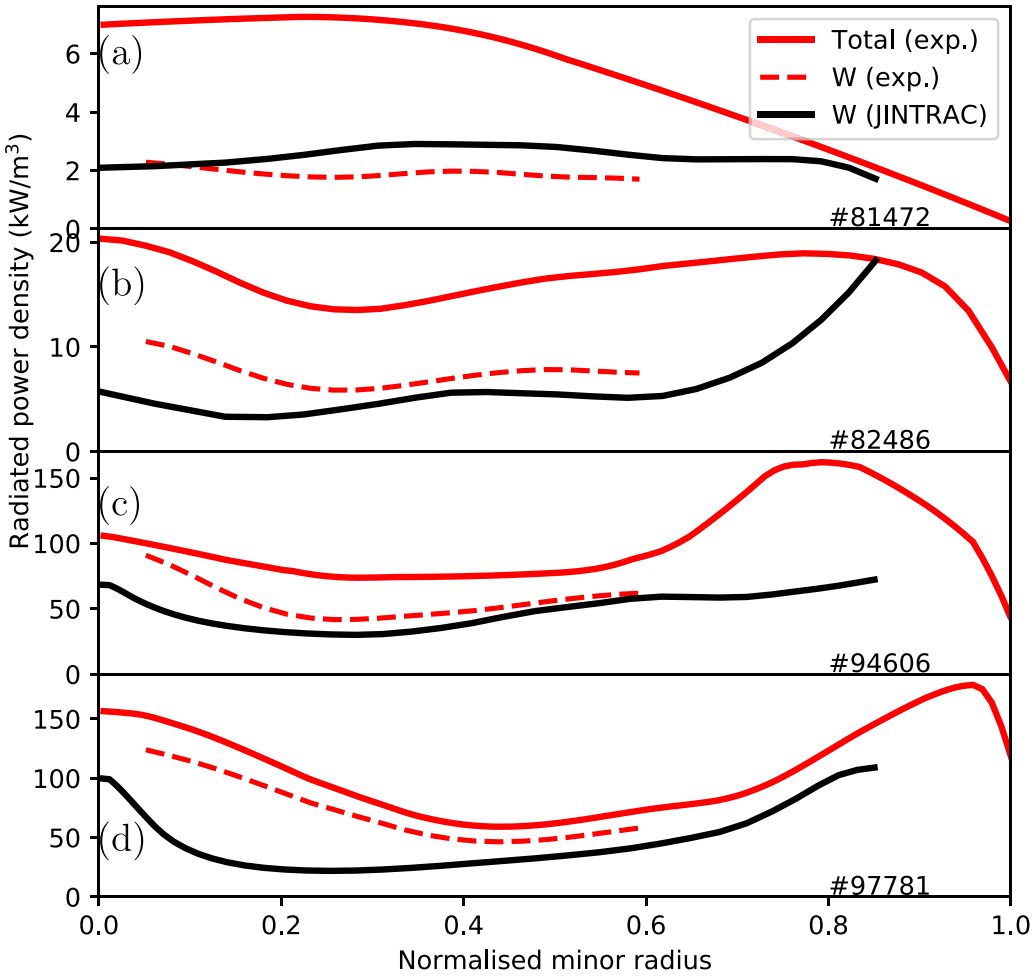

Figure 6. The flux-surface averaged total radiated power density (red solid lines) and the estimated contribution of W radiation (red dashed lines) based on an integrated data analysis. [9] of core diagnostics, and the W radiation predicted by JINTRAC (black) as a function of the normalised minor radius. The JET-ILW discharges shown are (a) L-mode #81 472 at 9 s, (b) ELMy H-mode #82 486 at 14 s, (c) ELMy H-mode #94 606 at 10 s, and (d) hybrid ELMy H-mode #97 781 at 9 s.

The measured heat and particle fluxes carried by individual ELMs, occurring in experiments at quasiregular intervals, are a source of uncertainty which affects the predictions of both W erosion and transport. The presented simulations assume that every ELM is described by the same JINTRAC plasma solution and that the ELM frequency is constant. In addition, modelling the temporal dynamics of the ELM cycle using 3–4 snapshots of the time-dependent JINTRAC simulation is unlikely to result in the same predicted W density as a hypothetical fully coupled JINTRAC-ERO2.0 simulation with plasma conditions updated each time step. Nevertheless, parameter sensitivity studies indicate that the inter-ELM core and pedestal plasma profiles are a larger source of uncertainty than the ELM dynamics.

Additional uncertainties in the predicted W erosion rate are introduced by the SDTrimSP sputtering yield data as well as statistical Monte Carlo noise in the calculations of the flux and energy spectrum of impacting particles at each wall location. The uncertainty of the W erosion rate predicted at a specific location is several times higher than the same uncertainty integrated over the area of one or more plasma-facing components, due to the difference in sample size.

The predicted W density on the closed flux surfaces has a non-negligible but weaker-than-linear inverse dependence on the magnitude of main ion flow in the SOL. The flow pattern in the SOL predicted by EDGE2D-EIRENE is more consistent with analysis of measurements [26] when the cross-field drifts are included than when the drifts are neglected. In the studied inter-ELM H-mode scenario with drifts (#94 606, $P_{\mathrm{aux}} = 18$ MW), the higher predicted flow velocity in the main chamber SOL results in a modest $<30\%$ reduction in the W density inside the separatrix, compared to the no-drift simulation.

Combining the aforementioned sources of modelling uncertainty, it is expected that the described W erosion and transport simulations can predict the W density profile within a factor of 3 in most cases when the simulated plasma conditions are thoroughly validated against measurements (table 2). The observed level of code-experiment agreement in the studied scenarios (factor of 2 to 3) supports the estimated modelling

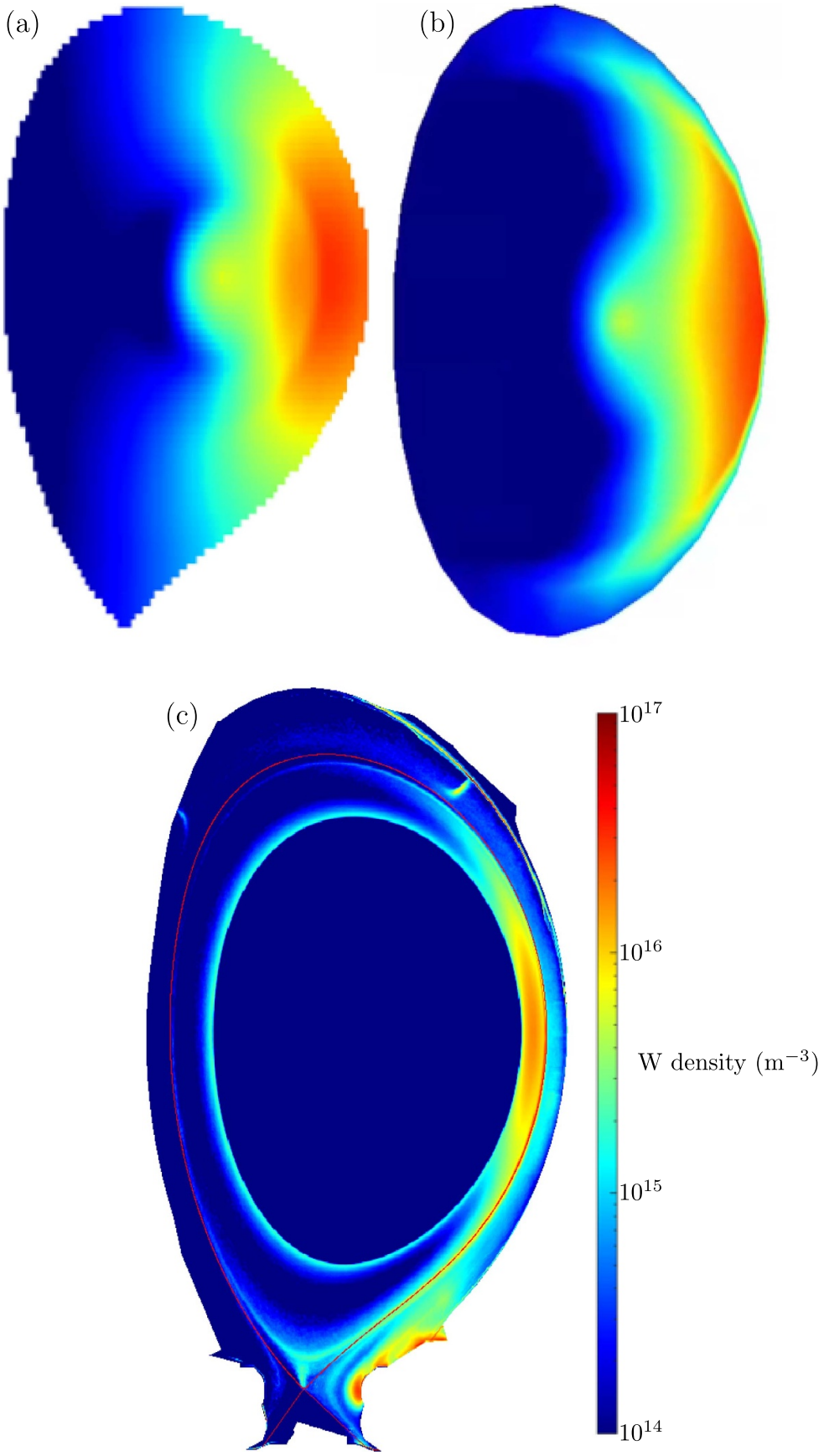

Figure 7. Poloidal cross-sections of the W density profile in JET-ILW discharge #97 781 at 9 s, (a) inferred from the experiment [9], (b) predicted by JINTRAC (NEO and QLK-NN) in the core plasma with a boundary condition from ERO2.0, and (c) ELM-averaged prediction for the edge plasma by ERO2.0.

Table 2. Non-exhaustive list of estimated significant sources of modelling uncertainty affecting the predicted W density. The estimates are case-specific and approximate. Informed guesses which are not derived from quantitative data are indicated with an asterisk (*). The uncertainties are propagated assuming a log-normal stochastic process (non-negative W density) and independent variables.

Measured or imposed simulation parameter	Relative st.dev. (σ/μ)	Impact on W density
Flux of energetic atoms incident on W tiles	+/−40%*	+/−40%*
T_e and n_e in the upstream scrape-off layer	+/−15%	+50%/−25%
H-mode pedestal T_i and n_e gradients	+/−15%	+35%/−30%
Core T_i and n_e gradients	+/−10%	+20%/−15%
Plasma rotation frequency profile	+/−15%	+15%/−10%
ELM amplitude and frequency	+/−20%	+15%/−30%
Time resolution of ELM conditions in ERO2.0		+/−25%*
Divertor surface morphology (smooth assumed)		−30%*
SOL flows induced by cross-field drifts	+100%	−25%
Approximate one-σ uncertainty, core W density		$\sim +\mathbf{94\%}/-\mathbf{71\%}$

uncertainty. In scenarios with scarce or unavailable measurement data, such as simulated future devices, the uncertainty of the predicted W density may be several times larger due to uncertain background plasma profiles.

5. Conclusions

A novel simulation workflow utilising ERO2.0 and JINTRAC is described and validated for improved prediction accuracy of W erosion and transport in the edge and core plasma. The predicted W density profiles in all studied L-mode and ELMy H-mode scenarios reproduce the experiment within a factor of 2 to 3, consistent with the estimated modelling uncertainty.

Carefully adjusting the plasma conditions (especially the n_e, T_i, T_e, and toroidal rotation profiles) to measurements is critical to the W prediction accuracy. To predict the W density in unexplored plasma scenarios or future devices without available plasma measurements, accurate and reliable predictive capabilities of the plasma conditions are also necessary. With a sufficiently valid treatment of W erosion and transport, the main limiting factors for W prediction accuracy are measurement and/or modelling uncertainties of the background plasma, as opposed to simplifications in the transport model.

Data availability statement

The data cannot be made publicly available upon publication because they are not available in a format that is sufficiently accessible or reusable by other researchers. The data that support the findings of this study are available upon reasonable request from the authors.

Acknowledgment

This work has been carried out within the framework of the EUROfusion Consortium, funded by the European Union via the Euratom Research and Training Programme (Grant Agreement No 101052200—EUROfusion). Views and opinions expressed are however those of the author(s) only and do not necessarily reflect those of the European Union or the European Commission. Neither the European Union nor the European Commission can be held responsible for them. The ERO2.0 simulations utilised computing resources provided by the Science-IT project at Aalto University.

ORCID iDs

H A Kumpulainen https://orcid.org/0000-0003-1301-0497
M Groth https://orcid.org/0000-0001-7397-1586
S Brezinsek https://orcid.org/0000-0002-7213-3326
F Casson https://orcid.org/0000-0001-5371-5876
L Frassinetti https://orcid.org/0000-0002-9546-4494
J Romazanov https://orcid.org/0000-0001-9439-786X

References

[1] Bolt H *et al* 2004 *J. Nucl. Mater.* **329–333** 66–73
[2] You J H *et al* 2022 *Fusion Eng. Des.* **175** 113010
[3] Pütterich T, Neu R, Dux R, Whiteford A D, O'Mullane M G and Summers H P 2010 *Nucl. Fusion* **50** 025012
[4] Brezinsek S *et al* 2019 *Nucl. Fusion* **59** 096035
[5] Kumpulainen H A, Groth M, Corrigan G, Harting D, Koechl F, Jaervinen A E, Lomanowski B, Meigs A G and Sertoli M 2020 *Nucl. Mater. Energy* **25** 100866
[6] Kumpulainen H A *et al* 2022 *Nucl. Mater. Energy* **33** 101264
[7] Köchl F *et al* 2016 *26th IAEA Fusion Energy Conf.*
[8] Casson F *et al* 2020 *Nucl. Fusion* **60** 066029
[9] Sertoli M, Carvalho P J, Giroud C and Menmuir S 2019 *J. Plasma Phys.* **85** 905850504
[10] Di Genova S *et al* 2023 *Nucl. Mater. Energy* **34** 101340
[11] Fajardo D, Angioni C, Casson F J, Field A R, Maget P and Manas P 2023 *Plasma Phys. Control. Fusion* **65** 035021
[12] Ho A, Citrin J, Bourdelle C, Camenen Y, Casson F J, van de Plassche K L and Weisen H 2021 *Phys. Plasmas* **28** 032305
[13] Romanelli M *et al* 2014 *Plasma Fusion Res.* **9** 3403023
[14] Simonini R, Corrigan G, Radford G, Spence J and Taroni A 1994 *Contrib. Plasma Phys.* **34** 368–73
[15] Wiesen S 2006 EDGE2D-EIRENE interface report (available at: www.eirene.de/e2deir_report_30jun06.pdf)
[16] Belli E A and Candy J 2008 *Plasma Phys. Control. Fusion* **50** 095010
[17] Bourdelle C, Garbet X, Imbeaux F, Casati A, Dubuit N, Guirlet R and Parisot T 2007 *Phys. Plasmas* **14** 112501
[18] Romazanov J *et al* 2019 *Nucl. Mater. Energy* **18** 331–8
[19] Mailloux J *et al* 2022 *Nucl. Fusion* **62** 042026

[20] Den Harder N *et al* 2016 *Nucl. Fusion* **56** 026014
[21] Homma Y *et al* 2012 *J. Comput. Phys.* **231** 3211–27
[22] Erba M, Cherubini A, Parail V V, Springmann E and Taroni A 1997 *Plasma Phys. Control. Fusion* **39** 261
[23] Houlberg W A, Shaing K C, Hirshman S P and Zarnstorff M C 1997 *Phys. Plasmas* **4** 3230
[24] Field A *et al* 2023 *Nucl. Fusion* **63** 016028
[25] Breton S, Casson F J, Bourdelle C, Angioni C, Belli E, Camenen Y, Citrin J, Garbet X, Sarazin Y and Sertoli M 2018 *Phys. Plasmas* **25** 012303
[26] Erents S K, Chankin A V, Matthews G F and Stangeby P C 2000 *Plasma Phys. Control. Fusion* **42** 905